

# Nanoimprinted ultrafine line and space nanogratings for liquid crystal alignment

Yan Jun Liu<sup>1</sup>, Wei Wei Loh<sup>1</sup>, Eunice Sok Ping Leong<sup>1</sup>,  
Tanu Suryadi Kustandi<sup>1</sup>, Xiao Wei Sun<sup>2</sup> and Jing Hua Teng<sup>1</sup>

<sup>1</sup> Institute of Materials Research and Engineering, Agency for Science Technology and Research (A\*STAR), 3 Research Link, Singapore 117602, Singapore

<sup>2</sup> School of Electrical and Electronic Engineering, Nanyang Technological University, Nanyang Avenue, Singapore 639798, Singapore

E-mail: [liuy@imre.a-star.edu.sg](mailto:liuy@imre.a-star.edu.sg)

Received 20 August 2012

Published 23 October 2012

Online at [stacks.iop.org/Nano/23/465302](http://stacks.iop.org/Nano/23/465302)

## Abstract

Ultrafine 50 nm line and space nanogratings were fabricated using nanoimprint lithography, and were further used as an alignment layer for liquid crystals. The surface morphologies of the nanogratings were characterized and their surface energies were estimated through the measurement of the contact angles for two different liquids. Experimental results show that the surface energies of the nanogratings are anisotropic: the surface free energy towards the direction parallel to the grating lines is higher than that in the direction perpendicular to the grating lines. Electro-optical characteristics were tested from a twisted nematic liquid crystal cell, which was assembled using two identical nanogratings. Experimental results show that such a kind of nanograting is promising as an alternative to the conventional rubbing process for liquid crystal alignment.

(Some figures may appear in colour only in the online journal)

## 1. Introduction

Alignment is a crucial step in the fabrication of high-quality liquid crystal displays (LCDs). Conventionally, liquid crystals (LCs) are aligned by mechanically rubbing the surface of polyimide films, and this method is widely used for commercial displays because it is a parallel and low cost process [1]. However, the rubbing method has very limited control of the alignment properties and introduces impurities and dust into the fabrication process. To overcome these issues, a number of alignment methods have been proposed as potential replacements for the rubbing process, such as the oblique evaporation method [2], the photoalignment method [3–5], and ion beam alignment methods [6–9]. However, these methods are rarely cost-effective due to complexity. Alternatively, according to Berreman's groove theory [10], LC molecules can also be aligned by employing specific surface topographies, such as microgrooves [11–13], and surface relief gratings [14, 15]. The alignment of LC molecules by microscale or nanoscale patterns allows more freedom in the control of alignment properties

(i.e. pretilt angle, anchoring energy, and multistability) than conventional methods. Upon the pattern fabrication, nanoimprinting lithography (NIL) [16–19] and holographic patterning [20–23] stand out in terms of easy fabrication, large area patterning, mass production, and cost effectiveness. In addition, both techniques can produce smaller and deeper patterns than surface relief and photoalignment methods. However, the pitch of the holographic pattern strongly depends on the laser wavelength, hence limiting the minimum pitch to be  $\sim\lambda/2$ . In contrast, advances in NIL technology make it possible to produce much finer patterns ( $\sim 10$  nm), hence attracting intense interest for alignment of LCs.

In the past few years, researchers have exploited NIL technology to create two different methods for LC alignment. One way is to generate nanoscale polymeric surface grooves on substrates based on NIL for the LC alignment [24–28]. The other way is to fabricate nanoscale grating patterns with indium–tin–oxide (ITO) and indium–zinc–oxide (IZO) by an ultraviolet nanoimprint technique and sputter deposition process as conducting electrodes for LC devices [29, 30]. Furthermore, since LCs can be well aligned

on imprinted patterns, different tunable photonic devices, such as filters [31] and lasers [32], have been developed based on NIL technology.

In this paper we have investigated LC alignment using an ultrafine line and space (L&S) nanograting pattern formed by NIL. We have experimentally confirmed that LC molecules can be aligned using this topographic pattern through the measurements of the electro-optical behavior of the LC molecules. This technique is expected to be very useful for achieving convenient and uniform alignment of LC molecules.

## 2. Experiments

### 2.1. Nanograting fabrication

A step and flash imprinting process was performed using Imprio 100 (Molecular Imprints, Inc.). Before the imprinting process, an indium–tin oxide (ITO) layer of ~100 nm was coated on one side of a double-side polished sapphire substrate in order to investigate the electro-optical properties of the devices. An organic material (Transpin HE-0600, Molecular Imprints, Inc.) was then spun onto the ITO surface of the substrate at two-step spin-speeds: 1800 rpm for 3 s and 3000 rpm for 30 s, and baked at 195 °C for 5 min to obtain a 65 nm thick planarization layer. Liquid acrylate imprint resist, poly(methyl methacrylate) (PMMA), was subsequently dispensed across the surface of the sapphire substrate. A quartz template, with a size of 65 mm × 65 mm and 10 mm × 10 mm active patterned area, was lowered until contact is made with the imprint resist, and capillary action induces the liquid imprint resist to completely fill the region between the substrate and the topography of the imprint template. Fabrication of the quartz template was realized using a conventional electron beam lithography and etching process. The quartz template featured 50 nm line and space structures (duty ratio of 1) with a height of 100 nm and a pitch of 100 nm. Following the imprint process, the imprint resist was photopolymerized via ultraviolet illumination, after which the template was separated from the substrate, leaving behind an exact inverse replica of the template pattern. This imprint process can be repeated across the substrate areas to obtain several imprint fields on the substrate.

### 2.2. Liquid crystal infiltration

Once the imprinted nanograting samples are ready, a twisted nematic (TN) cell was formed by assembling two nanograting samples with the grating lines orthogonally arranged. The cell thickness was controlled to be ~7 μm using polystyrene microbeads. The LC material used in our experiments was a nematic LC, E7 (Merck), which has an ordinary refractive index of  $n_o = 1.521$  and an extraordinary refractive index of  $n_e = 1.746$ , giving a birefringence of  $\Delta n = 0.225$  (all at  $\lambda = 589$  nm). The LC in the isotropic phase was infiltrated into the LC cell by a capillary action at a temperature of 65 °C, which is above the clearing point (58 °C) of LC E7. After infiltration, the LC cell was cooled down naturally to room temperature for optical and electro-optical characterization.

### 2.3. Characterization

The surface morphologies of the nanogratings were characterized using scanning electron microscopy (SEM) and atomic force microscopy (AFM). The contact angle of the nanograting surface was measured by a contact angle goniometer (Ramé-Hart) and was further analyzed with DROPImage advanced software. Optical transmittance of the TN LC cell was measured at room temperature using a UV–vis–NIR microspectrophotometer (CRAIC QDI 2010<sup>TM</sup>). Microscopic photographs were captured through a charge-coupled-device (CCD) camera built in the UV–vis–NIR microspectrophotometer. Transmittance versus voltage characteristics were measured using a He–Ne laser (633 nm), a power meter, and a function generator. The TN LC cell was placed in between two parallel polarizers with one polarizer optical axis parallel to the nanograting lines. A rectangular waveform with a frequency of 1 kHz was applied to the TN LC cell.

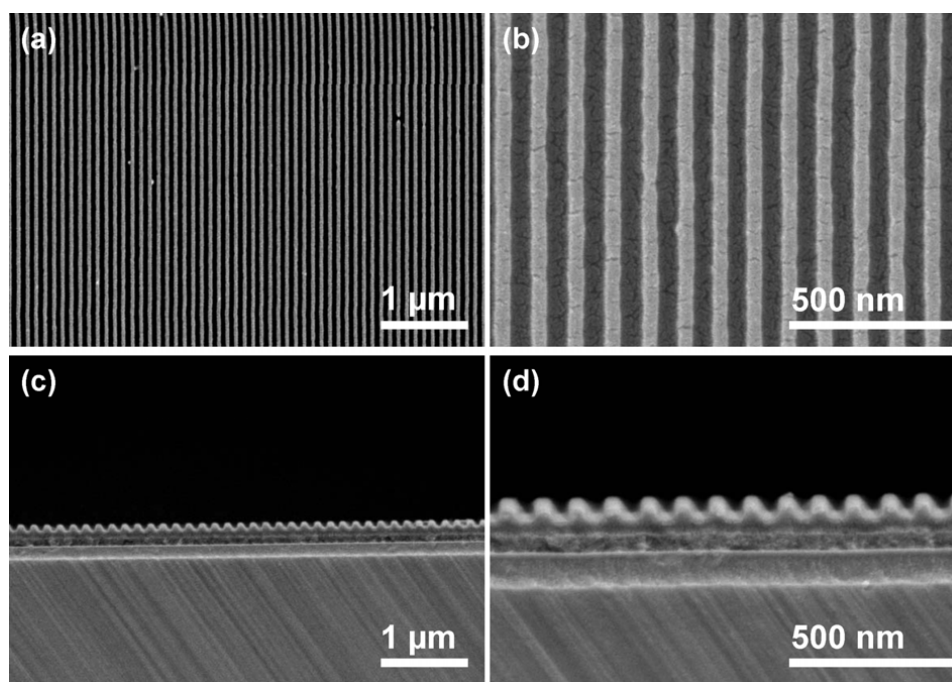
## 3. Results and discussion

Figure 1 shows SEM images of the PMMA nanogratings after NIL. A clear L&S patterns was realized. The pitch (sum of the widths of a trench and a ridge) of the L&S pattern is 100 nm. The duty ratio of line to space is ~0.9, which is slightly smaller than that of the quartz template. The decrease of the duty ratio is reasonable since the photopolymerization of PMMA generally induces shrinkage in volume. From figure 1(d), we can also note that the PMMA wall shapes of the L&S pattern did not ideally inverse-replicate the template pattern and a bell-bottomed structure was obtained in our experiment. There are two possible reasons why such a structure was formed: (1) PMMA did not enter into the corners of the grooved pattern because the spacing was very narrow, and (2) a residual layer of PMMA layer existed at the bottom of the imprinted structure. Furthermore, we characterized the surface morphologies using AFM, as shown in figure 2(a). The measured depth of these wells is only ~15 nm on average, as shown in figure 2(b), which is much smaller than the (100 nm) of the mold. This further confirms that the PMMA did not fill the trench of the mold completely. However, according to the microgroove theory [10], such a nanograting with a pitch and step height of 100 and 15 nm is sufficient to align the LC molecules.

Contact angles and surface energies were also measured to investigate the effect of nanograting alignment. These parameters can provide an indication of the chemical affinity of the surfaces studied. Owens and Wendt have developed a method to approximate the surface free energy of solids, especially for polymers, based on the measurement of contact angles [33]. The relation between the contact angle and the surface free energy is as follows:

$$1 + \cos \theta = 2\sqrt{\gamma_s^d} \left( \frac{\sqrt{\gamma_1^d}}{\gamma_1} \right) + 2\sqrt{\gamma_s^h} \left( \frac{\sqrt{\gamma_1^h}}{\gamma_1} \right) \quad (1)$$

where  $\gamma_1 = \gamma_1^d + \gamma_1^h$  and  $\gamma_s = \gamma_s^d + \gamma_s^h$  are the surface free energies of a given liquid and solid, respectively, which are



**Figure 1.** SEM images of top ((a) and (b)) and cross-sectional ((c) and (d)) views with different magnifications for the PMMA nanogratings.

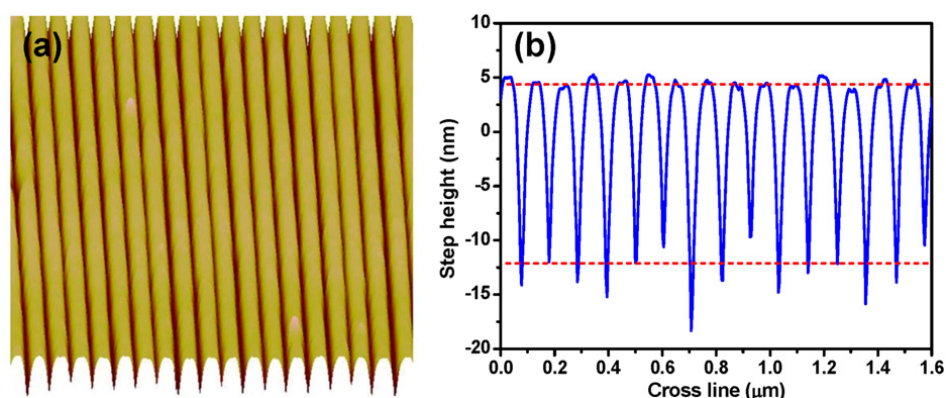


**Figure 2.** 3D view of the AFM image (a) and measured step height of the nanogratings (b).

the sums of contributions from the different intermolecular forces at the surface, the superscripts h and d refer to the hydrogen bonding and dispersion force components. Since many liquids have known values of  $\gamma_1^d$  and  $\gamma_1^h$ , by measuring the contact angle  $\theta$  of two different liquids against a solid we can obtain simultaneous equations to be solved for  $\gamma_s^d$  and  $\gamma_s^h$ . As a result, the components of surface free energy for a solid due to various forces can be approximated, and the sum of these components therefore gives a reasonable approximation of the total solid surface energy  $\gamma_s$ . In our measurement, the surface energies were estimated from de-ionized (DI) water and glycerol. Figure 3 shows static contact angles of DI water and glycerol droplets on the PMMA nanograting surface along two directions: parallel and perpendicular to the grating lines. From figure 3, the nanograting surface shows obvious anisotropic wettability. The direction parallel to the

grating lines is much more wettable than that perpendicular to the grating lines. Table 1 summarizes the results of the measured contact angles of DI water and glycerol, and estimated surface energies for the imprinted nanograting surfaces along those two directions. From table 1, the measured contact angles markedly changed for DI water and glycerol; due to the anisotropic wettability of the imprinted nanograting surface, the contact angles for both liquids show a huge difference ( $>20^\circ$ ) along different directions. As a result, the estimated surface free energy of the imprinted nanograting is also anisotropic: for our case, the surface free energy towards the direction parallel to the grating lines was higher than that in the direction perpendicular to the grating lines, which similarly happens for most rubbed polyimide surfaces [34]. In most previous reports involving the rubbing process, the change in chemical affinity of the surfaces is

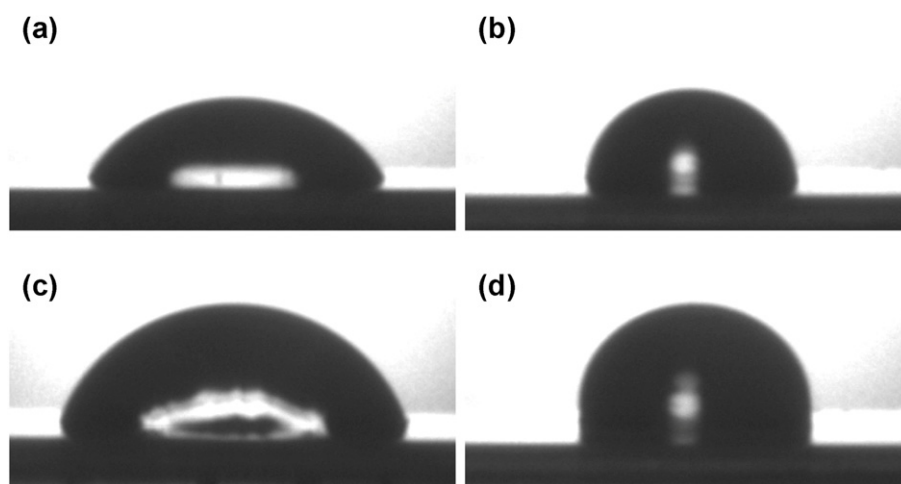


**Figure 3.** Static contact angles of DI water ((a) and (b)) and glycerol ((c) and (d)) droplets on the PMMA nanograting surface along two directions: parallel ((a) and (c)) and perpendicular ((b) and (d)) to the grating lines.

**Table 1.** Measured contact angles of DI water and glycerol, and estimated surface energies for the imprinted nanograting surfaces with two directions: parallel and perpendicular to the grating lines.

Nanograting	$\theta_{\text{DI-water}}$ (deg)	$\theta_{\text{Glycerol}}$ (deg)	$\gamma_1^d$ ( $\text{mJ m}^{-2}$ )	$\gamma_s^h$ ( $\text{mJ m}^{-2}$ )	$\gamma_s$ ( $\text{mJ m}^{-2}$ )
Parallel	64.5	70.6	1.4	42.4	43.8
Perpendicular	88.5	99.4	-0.7	33.6	32.9

attributed to the realignment of polymer chains. We also note that the nanoimprint process may induce a preferential alignment for some special molecules [35, 36]. However, in our nanoimprinted process, the polymer chains have no preferential alignment. Therefore, we attributed the chemical affinity to the surface topography, which subsequently induces uniform alignment of LC molecules.

Since transparency is the most important factor in the application of nanopatterned substrates to alignment layers, the optical transmittance at 300–900 nm was measured at room temperature. Figure 4 shows the measured transmittance of the as-deposited ITO on a sapphire substrate, the imprinted nanograting on top of the ITO layer, and the as-assembled LC cell after LC infiltration. Over the wavelength range 420–780 nm, the average optical transmittances of both bare ITO sapphire and the nanoimprinted layer were above 90%, showing an excellent transparency. The largest transmittance loss of only about 5% was observed at 550 nm due to light scattering when light passes through the nanograting structure. However, this slight difference in the transparency of the bare ITO sapphire and nanogratings is negligible. More importantly, the assembled LC cell with such nanogratings still shows almost constant transmittance of ~83%, indicating that it is highly suitable for display applications. It is worth mentioning that there is a dramatic drop in transmittance below 400 nm after LC infiltration, which is due to the intrinsic absorption of the LC material.

Electro-optical properties were investigated to examine the potential of a nanoimprint technique for LCD applications.

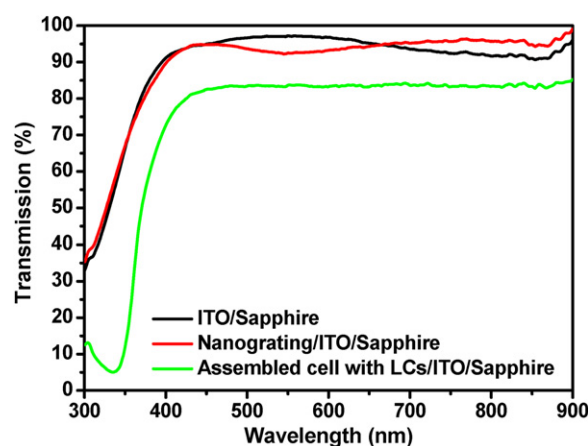


**Figure 4.** Measured transmittance of the as-deposited ITO on sapphire substrate, the imprinted nanograting on top of ITO layer, and the as-assembled LC cell after LC infiltration.

Using the nanograting alignment layer, a TN cell was fabricated. The lines of nanogratings on both substrates were perpendicular to each other, and the cell gap was about  $7 \mu\text{m}$ . Figure 5 shows the dynamic changes of transmission when a driving voltage was applied to the LC cell. From figure 5, the threshold voltage of the TN LC cell was  $\sim 4 \text{ V}$ . The transmission saturated at about 10 V. The achieved contrast ratio was  $\sim 38$ .

The insets in figure 5 show the captured photographs of the TN LC cell under different voltages between parallel polarizers. In the off state, LC molecules remain parallel to the nanograting lines, hence forming a  $90^\circ$  twist. Light transmission is therefore prohibited between parallel polarizers, resulting in a dark image (inset I). When a voltage is applied to the cell (on state), LC molecules start to gradually align along the electric field direction. At the fully switching voltage (10 V in this case), most LC molecules will completely align along the electric field direction, i.e. perpendicular to the nanograting surface, and the LC cell shows highest transmittance, resulting in a white image

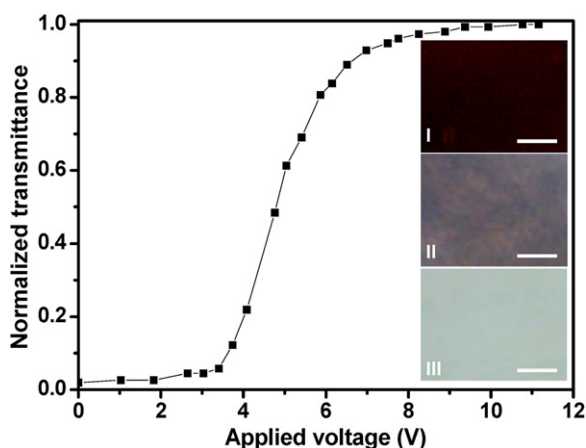


**Figure 5.** Dynamic transmission changes of the LC cell under different driving voltages. Insets show photographs of the TN LC cell under different voltages between parallel polarizers. Scale bar is 200  $\mu\text{m}$ .

(inset III). In between, the LC cell shows an intermediate transparency. Inset II shows the case when a threshold voltage was applied to the cell, where partial LC molecules just start to align along the electric field direction. From the inset photographs, uniform alignment was also confirmed for the TN LC cell.

As a final remark, we comment on how to further improve the performance of a nanograting-based TN LC cell in the following two aspects. First, the threshold could be further decreased by minimizing the surface energy of the nanogratings. This could be achieved by optimizing the pattern structures (pitch and height). A further surface treatment, for instance, removal of the PMMA residual layer by oxygen plasma etching, would also benefit the decrease of the nanograting surface energy. Second, the contrast ratio could also be further increased by optimizing the cell thickness. To improve the contrast ratio, the main concern is to achieve the minimum transmission, which can be achieved using a suitable cell thickness according to Gooch–Tarry’s minimum condition [37].

#### 4. Conclusion

In summary, we have demonstrated a twisted LC cell using a nanograting pattern as the alignment layer fabricated by NIL. Transmittance measurements for the nanograting layer on ITO coated glass showed that the transparency is sufficient for display applications. Furthermore, the nanograting-based LC cells showed a performance competitive with conventional LC cells. Twisted LC alignment was achieved inside the LC cell, where the two nanogratings are orthogonally arranged. The surface energy of the PMMA nanograting was estimated through contact angle measurements of two liquids: DI water and glycerol. Electro-optical performance of the nanograting-based LC cell was comparable to that of a rubbed polyimide cell. Therefore, this proposed approach is expected to be applicable as an alternative to the conventional rubbing process for LC alignment.

#### Acknowledgment

This work was financially supported by Agency for Science, Technology and Research (A\*STAR), under grant nos 0921540099 and 0921540098.

#### References

- [1] Geary J M, Gooby J W, Kmetz A R and Patel J S 1987 *J. Appl. Phys.* **62** 4100
- [2] Janning J L 1972 *Appl. Phys. Lett.* **21** 173
- [3] Gibbons W M, Shannon P J, Sun S and Swetlin B J 1991 *Nature* **351** 49
- [4] Ichimura K 2000 *Chem. Rev.* **100** 1847
- [5] Fuh Y-G, Liu C-K, Cheng K-T, Ting C-L, Chen C-C, Chao P C-P and Hsu H-K 2009 *Appl. Phys. Lett.* **95** 161104
- [6] Chaudhari P et al 2001 *Nature* **411** 56
- [7] Stohr J, Samant M G, Luning J, Callegari A C, Chaudhari P, Doyle J P, Lacey J A, Lien S A, Purushothaman S and Speidell J L 2001 *Science* **292** 2299
- [8] Oh B Y, Lee K M, Kim B Y, Kim Y H, Han J W, Han J M, Lee S K and Seo D S 2008 *J. Appl. Phys.* **104** 064502
- [9] Kang Y G, Park H G, Kim H J, Kim Y H, Oh B Y, Kim B Y, Kim D H and Seo D S 2010 *Opt. Express* **18** 21594
- [10] Berreman D W 1972 *Phys. Rev. Lett.* **28** 1683
- [11] Berreman D W 1973 *Mol. Cryst. Liq. Cryst.* **23** 215
- [12] Flanders D, Shaver D and Smith H 1978 *Appl. Phys. Lett.* **32** 15
- [13] Bryan-Brown G P, Brown C V, Sage I C and Hui V C 1998 *Nature* **392** 365
- [14] Behdani M, Keshmiri S H, Soria S, Bader M A, Ihlemann J, Marowsky G and Rasing T 2003 *Appl. Phys. Lett.* **82** 2553
- [15] Kim J Y, Kim T H, Kimura T, Fukuda T and Matsuda H 2003 *Opt. Mater.* **21** 627
- [16] Soloviev V S, Boiko Y B, Perlo P and Grover C P 2002 *Proc. SPIE* **4658** 137
- [17] Chou S Y, Crauss P R and Renstrom P J 1995 *Appl. Phys. Lett.* **67** 3114
- [18] Haisma J, Verheijen M, van den Heuvel K and van den Berg J 1996 *J. Vac. Sci. Technol. B* **14** 4124
- [19] Resnick D J, Sreenivasan S V and Willson C G 2005 *Mater. Today* **8** 32
- [20] Yew S Y, Kustandi T S, Low H Y, Teng J H, Liu Y J and Leong E S P 2011 *Microelectron. Eng.* **88** 2946
- [21] Crawford G P, Eakin J N, Radcliffe M D, Callan-Jones A and Pelcovits R A 2005 *J. Appl. Phys.* **98** 123102
- [22] Liu Y J and Sun X W 2006 *Appl. Phys. Lett.* **89** 171101
- [23] Liu Y J, Zheng Y B, Shi J, Huang H, Walker T R and Huang T J 2009 *Opt. Lett.* **34** 2351
- [24] Liu Y J, Dai H T and Sun X W 2011 *J. Mater. Chem.* **21** 2982
- [25] Yi Y, Nakata M, Martin A R and Clark N A 2007 *Appl. Phys. Lett.* **90** 163510
- [26] Gwag J S, Oh-e M, Yoneya M, Yokohama H, Satou H and Itami S 2007 *J. Appl. Phys.* **102** 063501
- [27] Gwag J S, Kim J-H, Yoneya M and Yokoyama H 2008 *Appl. Phys. Lett.* **92** 153110
- [28] Gwag J S, Oh-e M, Kim K-R, Cho S-H, Yoneya M, Yokohama H, Satou H and Itami S 2008 *Nanotechnology* **19** 395301
- [29] Takahashi H, Sakamoto T and Okada H 2010 *J. Appl. Phys.* **108** 113529
- [30] Kim H J, Kim H G, Kim K, Park S-H, Gim M-J, Jang J-J, Choi S-W and Kim S S 2010 *Mol. Cryst. Liq. Cryst.* **530** 7/[163]

- [30] Kim H J, Lee J G, Kim H G, Choi S-W and Kim S S 2010 *Japan. J. Appl. Phys.* **49** 024207
- [31] Chang A S P, Morton K J, Tan H, Murphy P F, Wu W and Chou S Y 2007 *IEEE Photon. Technol. Lett.* **19** 1457
- [32] Ozaki R, Shinpo T, Yoshino K, Ozaki M and Moritake H 2008 *Appl. Phys. Express* **1** 012003
- [33] Owens D K and Wendt R C 1969 *J. Appl. Polym. Sci.* **13** 1741
- [34] Zheng W 2010 Surface wetting characteristics of rubbed polyimide thin films *Polymer Thin Films* ed Hashim A A (Rijeka: InTech) chapter 10
- [35] Wang J, Sun X Y, Chen L, Zhuang L and Chou S Y 2000 *Appl. Phys. Lett.* **77** 166
- [36] Chiu C-H, Kuo H-L, Chen P-C, Wen C-H, Liu Y-C and Chen H-M P 2006 *Appl. Phys. Lett.* **88** 073509
- [37] Gooch C H and Tarry H A 1975 *J. Phys. D: Appl. Phys.* **8** 1575